Journal of Dynamics, Monitoring and Diagnostics, 2026, 5, 106-116
https://doi.org/10.37965/jdmd.2026.1315

ISTP
RESEARCH ARTICLE

Adaptive Physics-Data Fusion for Data-Efficient Prognostics of Aircraft Hydraulic Filters

Dinghui Guo, Weijie Wang, and Yixuan Geng
College of Robotics Science and Engineering, Taiyuan University of Technology, Taiyuan 030024, China

(Received 06 April 2026; Revised 15 May 2026; Accepted 15 May 2026; Published online 18 May 2026)

Abstract: Due to the stringent cleanliness requirements of the aviation hydraulic system, predicting the health status of hydraulic filter is essential for ensuring flight safety. However, it is still a challenge to have an accuracy prediction due to complex physical degradation mechanisms and insufficient individual degradation data in early stage. Therefore, an adaptive physics-data fusion (APDF) model is proposed to predict hydraulic filter health status by integrating the advantages of physical and data information. Specifically, a parameter-updated Ergun equation, describing the pressure drop across the filter with the contaminant deposition, is taken as physical knowledge to guide the design of neural network structure and loss function. In addition, an adaptive weighting strategy in the loss function is also developed to dynamically balance the physical and data contributions. The experimental results from the hydraulic filter degradation experiment show that the model achieves a pressure drop prediction accuracy with root mean squared error of 0.0076 MPa. Notably, under limited data in the early prediction stage (only with 40% training data), the APDF represents 87.5% improvement compared to traditional data-driven models (such as long short-term memory). This performance highlights significant advantages in scenarios with limited aviation sensor configurations.

Keywords: adaptive weighting strategy; health status prediction; hydraulic filter; long short-term memory network; physics-informed neural network; prognostics and health management

I. INTRODUCTION

The hydraulic system plays a crucial role in aircraft operations, controlling the actuation of systems, such as the landing gear, braking system, and flight control surfaces [1]. The hydraulic filter is essential for maintaining hydraulic fluid cleanliness, as over 70% of hydraulic failures are caused by contamination from external particles and wear debris [2,3]. However, as operating time increases, the accumulation of contaminants in the filter leads to clogging degradation, significantly affect hydraulic system performance [4]. Therefore, predicting filter degradation accurately is essential for ensuring system safety, optimizing maintenance schedules, and preventing unplanned downtime [5].

In recent years, various prediction methods for the filter have been proposed, which can be broadly categorized into physics-driven method and data-driven method [6–9].

The physics-driven method applies fluid mechanics to characterize the flow dynamics within the hydraulic filter and the deposition process of contaminants [10]. Kozeny-Carman [11] and Ergun [12] equations are commonly used to model the pressure drop of fluid through a porous medium. Eker *et al.* [13] further introduced the effective filtration area ratio parameter and proposed a modified Ergun model to fully describe the entire lifecycle process of filter clogging. Although physics-driven method is generally reliable and stable, the incompleteness of the physic model in representing the degradation mechanisms, the complexity of the operating conditions, and the differences in individual degradation make it still challenging to precisely describe the degradation process for a specific hydraulic filter.

Corresponding author: Weijie Wang (e-mail: wangweijie@tyut.edu.cn).

Data-driven methods, such as multi-layer perceptron (MLP) [14] and long short-term memory (LSTM) [15] networks, directly learn degradation patterns from data without relying on specific physical mechanisms. Their superior learning capabilities enable effective capture of nonlinear degradation patterns and adaptation to individual variations [16]. Lee *et al.* [17] introduced a Health Index (HI) to assess the health status of filters and employed a bidirectional LSTM to predict the Remaining Useful Life (RUL). Tiltmann *et al.* [18] designed a CNN-GRU model that combines the feature extraction capability of 1D-CNN with the long-term dependency learning of GRU to predict the health status of filters.

However, the performance of data-driven approach relies heavily on abundant historical degradation data [19]. In practice, the degradation of filters exhibits significant uncertainty and individual variability, which limits the transferability of degradation patterns across filters. As a result, individual degradation data are more suitable for modeling and predicting the behavior of a specific filter. However, such data are often scarce, particularly in the early degradation stage [20–22], making it difficult to accurately characterize the complete degradation process. These constraints pose significant challenges for industrial applications, notably reducing prediction accuracy during the initial phase of degradation.

Considering that physics-driven method can describe the general degradation patterns of the filter, effectively integrating physics information with data-driven approaches has the potential to have a data-efficient prognostics of aircraft hydraulic filter, which can improve prediction accuracy under data-limited conditions [23–25]. In this study, an adaptive physics-data fusion (APDF) model is proposed for predicting the health status of aviation hydraulic filter. By embedding physical

information into the network architecture and loss function, a deep fusion of physical mechanisms and data characteristics is achieved.

The contributions of this paper are summarized as follows:

1. A physics-inspired network structure is constructed. Guided by the physical model, the input of the model is designed, and a parameter-updated physics feature extraction layer is embed. This design reduces the complexity of the model, making predictions more physically consistent and accurate.
2. A physics-informed loss function is designed by incorporating physical constraints based on the filter degradation mechanism. This enables the model to accelerate convergence and enhance generalization under limited data conditions.
3. An adaptive physical weighting mechanism is introduced to dynamically balance the contributions between physical and data-driven components during training. This adaptive strategy allows the model to automatically adjust its reliance on physical priors according to data quality and training stage, enhancing prediction robustness and accuracy.

The structure of this paper is as follows: Section II introduces the APDF model for health status prediction of aircraft hydraulic filter; Section III elaborates on the experimental bench design and model parameter set; and Result and discussion are given in Section IV.

II. APDF FRAMEWORK

A. HYDRAULIC FILTER DEGRADATION MECHANISM MODEL

The pressure drop across the filter element is chosen as the performance degradation indicator for the hydraulic filter [26]. The hydraulic filter clogging process can be divided into two stages based on the rate of change of pressure drop over time: the healthy stage and the degradation stage [13]. As shown in Fig. 2, during the healthy stage, the mesh aperture is much larger than the contaminant particles, resulting in little pressure drop and stable flow rate. In contrast, in the degradation stage, the accumulated contaminant particles form a significant filter cake layer on septum, leading to an increase in pressure drop. As the filter cake layer further grows to the spatial limit of the hydraulic filter, the lateral growth of the filter cake is inhibited, leading to a sharp decrease in the effective filtration area. Then, the pressure drop of the hydraulic filter exhibits an exponential growth trend. Traditionally, the portion of the pressure drop exceeding 1.1 times the initial minimum value is defined as the degradation phase [13].

In this study, an extended Ergun equation is introduced to describe the pressure drop mechanism as contaminated oil flowing through porous media. This equation establishes a relationship between the filter pressure drop and critical clogging parameters, such as effective filtration area, volumetric flow rate, filter cake thickness, and porosity:

$$P(t) = \frac{10AV_s\mu_T(1-\varepsilon)^2L}{D_p^2\varepsilon^3 a} + \frac{B(1-\varepsilon)\rho V_s^2 L}{\varepsilon^3 D_p a} \tag{1}$$

where $P(t)$ is the pressure drop across the filter, L is the thickness of the filter cake (clogging layer), ε is the porosity of the filter cake, V_s is the flow rate of the oil, and μ_T is the viscosity of the oil, which decreases as the temperature increases. D_p is the diameter of the contaminant particles, ρ is the density of the oil, a is the effective filtration area ratio, and A and B are constants in the model.

The thickness L of the filter cake in Eq. (1) gradually increases as contaminant particles accumulate on the surface of the filter septum. The empirical logarithmic clogging thickness model can serve as a quantitative result for the filter cake thickness and provides auxiliary information for modeling hydraulic filter degradation. This model has been validated in [11] based on a high-quality macro-lens camera and image processing techniques. It can be expressed as [11,13]:

$$L = \begin{cases} b_1 \ln(b_2(t+c_1)+1) + b_3, & t < t_c \\ h_{\max}, & t \geq t_c \end{cases} \tag{2}$$

where t is time, $h_{\max}$ is the depth of the filter chamber, and $\Delta_L = [b_1, b_2, b_3, c_1, t_c]$ are constants in the model.

The porosity ε in Eq. (1) can be defined as [11]:

$$\varepsilon = 1 - \frac{M(c)/\rho}{LA_f} \tag{3}$$

where $M(c)$ is the total mass of contaminant particles, c is the contamination concentration of the oil, $M(c)/\rho$ is the cumulative volume of contaminant particles, and A_f is the area of the filter cake.

The effective filtration area ratio a is defined as the ratio of the filtration area that the filter cake can pass through in the filter chamber to the initial value. At the beginning of filtration, the effective filtration area ratio remains at 1. As the cake height is restricted by the rigid wall of the filtration chamber and cannot continue to grow, the effective filtration area ratio will dramatically decrease. Based on the experiments and verifications in [13], the formula is given as follows:

$$a = \begin{cases} 1, & t < t_c \\ d_1 e^{-d_2 t} + d_3, & t \geq t_c \end{cases} \tag{4}$$

where $\Delta_a = [d_1, d_2, d_3]$ are constants in the model.

Taking derivative to Eq. (1), we obtain the rate of pressure drop change:

$$\begin{aligned} \frac{\partial P(t)}{\partial t} = & \frac{10AV_s\mu_T\varepsilon(1-\varepsilon)^2L' - (1-\varepsilon)(3-\varepsilon)L\varepsilon'}{D_p^2\varepsilon^3 a\varepsilon} \\ & + \frac{10AV_s\mu_T(1-\varepsilon)^2La'}{D_p^2\varepsilon^3 a^2} \\ & + \frac{B\rho V_s^2}{\varepsilon^3 D_p a}\left[\frac{(2\varepsilon-3)L\varepsilon'}{\varepsilon} + \frac{(\varepsilon-1)La'}{a} + (1-\varepsilon)L'\right] \end{aligned} \tag{5}$$

Therefore, the physical degradation mechanism model based on the Ergun equation can be expressed as:

$$\frac{\partial P(t)}{\partial t} = f(t, L, \varepsilon, V_s, \mu, a, \Delta) \tag{6}$$

where $\Delta = [A, B, \Delta_L, \Delta_a]$ represents the parameters in the mechanistic model that can be trained and updated, and the detailed update method is introduced in part 2.3.

B. PHYSICS-INSPIRED NEURAL NETWORK STRUCTURE FOR HYDRAULIC FILTER PRESSURE DROP PREDICTION

According to Eq. (5), it can be founded that flow rate V_s, temperature T, contaminant concentration c, and historical

pressure drop $P_h(t)$ are the key factors affecting filter degradation. Therefore, these four factors are selected to be neural network inputs.

Furthermore, based on the filter degradation model, these variables above influence the pressure drop by affecting dynamic variables such as filter cake thickness L, effective filtration area ratio a, and filter cake porosity ε. In this study, a physics-driven feature extraction layer is introduced, as illustrated in Fig. 1. The input data are first processed through this layer, which employs a least-squares estimation method based on the Ergun equation to estimate the dynamic parameters, including the filter cake thickness L, effective filtration area ratio a, and filter cake porosity ε. These estimated dynamic parameters are then used as inputs to the LSTM neural network to predict the future pressure drop of the hydraulic filter [27].

The LSTM neural network consists of three stacked LSTM layers, three dropout regularization layers, and a fully connected output layer. The core computational process is as follows:

(1) Based on the hydraulic filter degradation hidden state h_{t-1} at time $t-1$ and the input $x_t = (\varepsilon_t, L_t, a_t)$ at time t, information flow is controlled through a gating mechanism, including the the forget gate f_t, input gate i_t, candidate state $\tilde{C}_t$, and output gate o_t:

$$\begin{aligned} f_t &= \sigma(W_f \cdot [h_{t-1}, x_t] + b_f) \\ i_t &= \sigma(W_i \cdot [h_{t-1}, x_t] + b_i) \\ o_t &= \sigma(W_o \cdot [h_{t-1}, x_t] + b_o) \\ \tilde{C}_t &= \tanh(W_C \cdot [h_{t-1}, x_t] + b_C) \end{aligned} \tag{7}$$

where σ is the sigmoid activation function, and $W = (W_f, W_i, W_o, W_C)$ and $b = (b_f, b_i, b_o, b_C)$ are the weight matrix and bias term, respectively.

(2) The memory unit combines the outputs of the forget gate f_t and the input gate i_t to update the cell state C_t, thereby storing long-term memory of degradation features such as hydraulic filter pore clogging and filter cake growth. This update process is described by the following formula:

$$C_t = f_t \odot C_{t-1} + i_t \odot \tilde{C}_t \tag{8}$$

where $\odot$ represents element-wise multiplication and C_t is initialized as a zero vector.

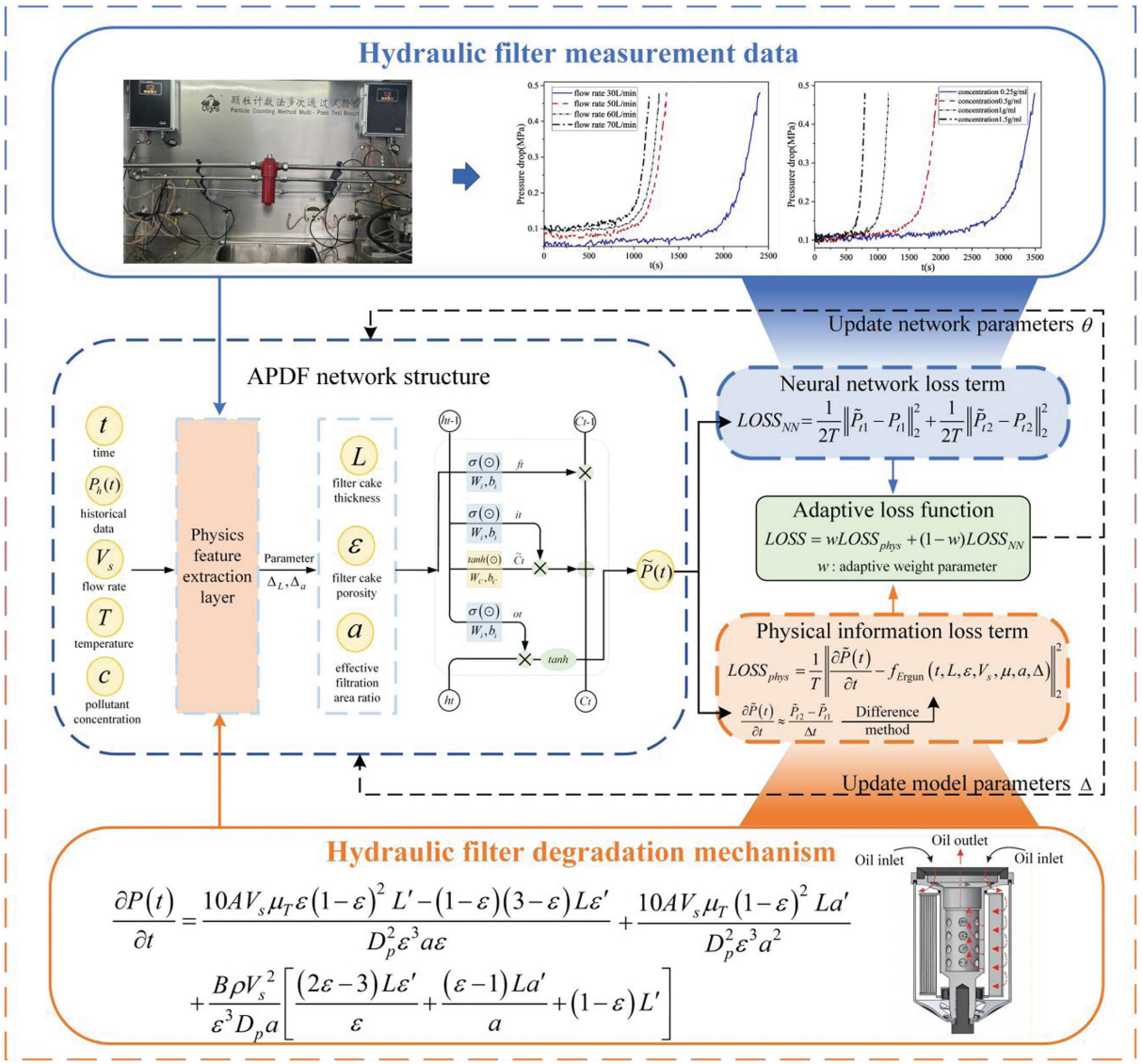

Fig. 1. The adaptive physics-data fusion (APDF) framework for health status prediction of aviation hydraulic filter.

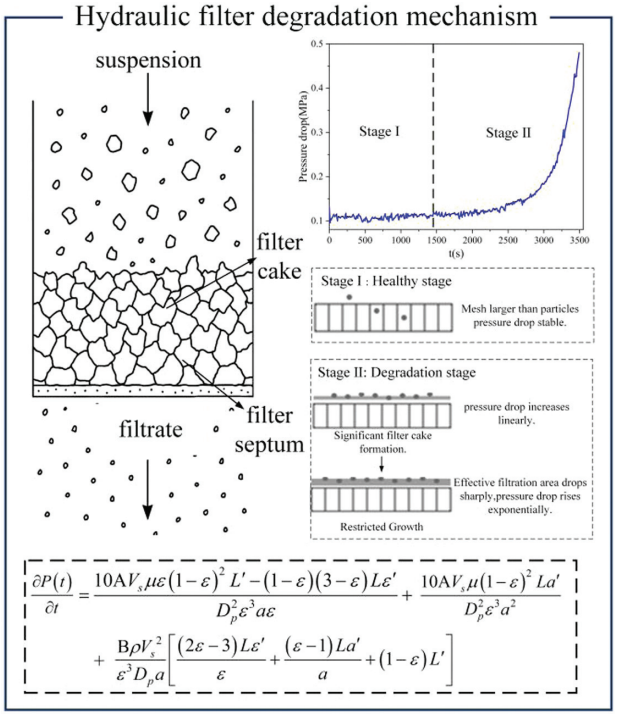

Fig. 2. Hydraulic filter degradation mechanism.

(3) Through the output gate o_t, the internal state information that stores the performance degradation characteristics of the hydraulic filter is transmitted to the external state h_t to encode the feature vector of the current time pressure drop, and the calculation process is as follows:

$$h_t = o_t \odot \tanh(C_t) \tag{9}$$

where the external state h_t is initialized as a zero vector.

C. PHYSICS-INFORMED LOSS FUNCTION

The loss function is the foundation of neural network training, defining the objective to be minimized and guiding the optimization of model parameters. Considering physical information has potential to guide the training of neural networks and narrow the search space of network parameters, we proposes a physics-informed loss function. From a broad perspective, it consists of two parts: the traditional neural network loss term $LOSS_{NN}$ and the physical information loss term $LOSS_{phys}$. The two parts are integrated through the adaptive weight. The loss function $LOSS$ of the APDF model can be expressed as:

$$LOSS = wLOSS_{phys} + (1-w)LOSS_{NN} \tag{10}$$

where w is the adaptive weight of the physical information loss term.

The loss function of the neural network $LOSS_{NN}$ can be calculated based on predicted values and measured values. The output of neural network contains two consecutive predicted values, expressed as $\widetilde{P} = (\widetilde{P}_{t1}, \widetilde{P}_{t2})$. The measured value at corresponding time are denoted as $P_{\text{real}} = (P_{t1}, P_{t2})$. The $LOSS_{NN}$ can be expressed as:

$$LOSS_{NN} = \frac{1}{2T}\left\|\tilde{P}_{t1} - P_{t1}\right\|_2^2 + \frac{1}{2T}\left\|\tilde{P}_{t2} - P_{t2}\right\|_2^2 \tag{11}$$

where T is the sampling time of measured data.

The loss function of the physical mechanism model $LOSS_{phys}$ can be calculated based on the predicted values and the extended Ergun equation as Eq (5). The physical information loss term $LOSS_{phys}$ can be defined as:

$$LOSS_{phys} = \frac{1}{T}\left\|\frac{\partial\tilde{P}(t)}{\partial t} - f(t,L,\varepsilon,V_s,\mu,a,\Delta)\right\|_2^2 \tag{12}$$

where $\frac{\partial\tilde{P}(t)}{\partial t}$ at time t can be calculated by the difference of the predicted pressure drop values in two future sample times which can be expressed as:

$$\frac{\partial\tilde{P}(t)}{\partial t} \approx \frac{\tilde{P}_{t2} - \tilde{P}_{t1}}{\Delta t} \tag{13}$$

where Δt is prediction time interval.

It is noteworthy that APDF introduces an adaptive weighting mechanism, which differs from the fixed weights in traditional PINN that are set based on expert experience. This design enables dynamic adjustment of the weights for physical constraints in the loss function, effectively balancing the learning of different physical constraints.

The key to training the APDF model is to minimize the gradients of the loss function with respect to both the neural network parameters θ and the parameters Δ of the physical model, while maximizing the adaptive weights w. The optimization objective is as follows:

$$\max_w \min_{\theta,\Delta} L(w,\theta,\Delta) \tag{14}$$

The gradient update algorithm is as follows:

$$\theta_{k+1} = \theta_k - \eta\frac{\partial LOSS}{\partial\theta_k} \tag{15}$$

$$\Delta_{k+1} = \Delta_k - \gamma\frac{\partial LOSS}{\partial\Delta_k} \tag{16}$$

$$w_{k+1} = w_k + \tau\frac{\partial LOSS}{\partial w_k} \tag{17}$$

where θ_k denotes the parameters of neural networks at the k-th step, Δ_k represents the physical parameters at the k-th step, w_k is the adaptive weight at the k-th step, and η, γ, and τ represent the learning rates.

However, simultaneous optimization of these three objectives may lead to training instability. Therefore, a stage-wise training strategy is adopted for the APDF model. First, the neural network is pretrained with physical parameters fixed at their initial values estimated by the least-squares method, and fixed weights are employed to combine loss terms, enabling the network to learn the basic patterns of the filter degradation. Subsequently, the joint optimization stage is entered, where both neural network parameters and physical parameters are updated simultaneously, with a smaller learning rate assigned to physical parameters to ensure their convergence to physically reasonable ranges. Finally, a gradient-based adaptive weighting mechanism is activated, which dynamically adjusts the weighting coefficients according to the relative magnitudes of gradients from different loss terms, thereby achieving automatic balancing of different optimization objectives.

The training process of the APDF model is shown in Algorithm 1:

Algorithm 1. APDF model training procedure.

Input:

-Training dataset $D = \{T_i, c_i, V_{si}, P_i\}_{i=1}^{N}$

-Initial neural network parameters θ; Physical model parameters Δ to be learned; Adaptive weights w

-APDF model hyperparameters: learning rate η, γ, τ, convergence threshold ξ

-Number of epochs E

Output:

-Trained APDF model parameters θ

-Trained DE model parameters Δ

-Trained adaptive weights w

for epoch = 1 to E **do**
  for each batch B in D **do**
    // Forward pass through APDF
    $\widehat{P}$ = APDF_forward (B,θ)
    // Calculate the total loss based on Eq. (9)
    $LOSS = w_1 LOSS_{NN} + w_2 LOSS_{phys}$
    // Backward pass to compute gradients
    $Gradients_{NN}$ = APDF_backward ($LOSS$,θ)
    $Gradients_{DE}$ = APDF_backward ($LOSS$,Δ)
    $Gradients_w$ = APDF_backward ($LOSS$,w)
    //stage 1: pre-training (fixed Δ and w)
    $\theta_{k+1} = \theta_k - \eta * Gradients_{NN}$
    //stage 2: Joint Optimization (fixed w)
    $\theta_{k+1} = \theta_k - \eta * Gradients_{NN}$
    $\Delta_{k+1} = \Delta_k - \gamma * Gradients_{DE}$
    //stage 3: Adaptive Weighting
    $\theta_{k+1} = \theta_k - \eta * Gradients_{NN}$
    $\Delta_{k+1} = \Delta_k - \gamma * Gradients_{DE}$
    $w_{k+1} = w_k + \tau * Gradients_w$
  end for
  if $LOSS < \xi$ **then**
    break
  end if
end for
return θ as the trained LSTM model parameters
return Δ as the trained DE model parameters
return w as the adaptive weights w

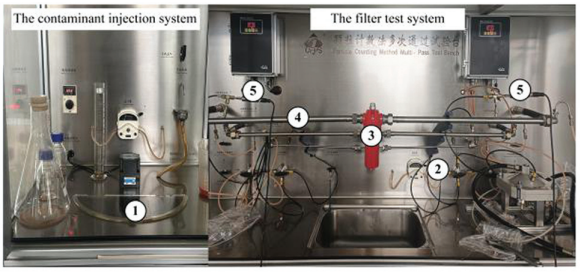

(a) Hydraulic filter experimental bench.

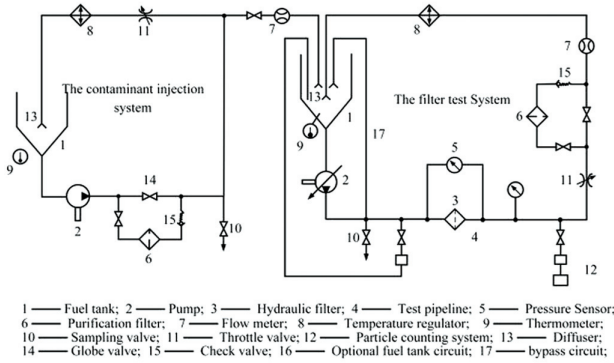

(b) Hydraulic schematic diagram of the filter experimental bench.

Fig. 3. Hydraulic filter degradation experiment bench.

III. EXPERIMENTAL STUDY

A. HYDRAULIC FILTER DEGRADATION EXPERIMENT SETTINGS

Degradation process of hydraulic filters was produced by a designed degradation experiment. As shown in Fig. 3, the experimental bench primarily consists of the hydraulic filter experimental system and the contaminant injection system.

The hydraulic filter experimental system consists of key components such as the oil tank, pump, test pipeline, pressure sensor, flow meter, and temperature sensor. These components provide the required oil flow and pressure for the system and enable real-time monitoring of parameters.

The contaminant injection system includes a storage tank for adequate contaminant supply, a stirring device for uniform dispersion, a fixed displacement pump for precise injection control, and an injection pipeline for targeted delivery. Based on these components, the contaminant load can be flexibly adjusted.

According to the working conditions of the aircraft hydraulic system, the flow rates in different flight phases are different [28]. Based on the analysis from [29], 30 L/min, 50 L/min, 60 L/min, and 70 L/min were selected as primary flow rates.

According to [30], the temperatures are mainly distributed between 30 °C and 50 °C. Therefore, 30 °C, 40 °C, and 50 °C were selected as the critical temperature conditions [27]. For contaminant concentration design, four different pollutant concentrations of 0.25 mg/L, 0.5 mg/L, 1 mg/L, and 1.5 mg/L were selected based on the national standard "Civil Aircraft Hydraulic Fluid Contamination Levels" [31]. The specific parameter configurations are detailed in Table I.

It should be noted that, to the best of our knowledge, there are currently no publicly available degradation datasets for hydraulic filters. The lack of such datasets significantly hinders the ability to model and predict hydraulic filter performance accurately. Although the degradation data collected in this study were obtained under fixed working conditions rather than dynamically varying ones, they still capture the essential degradation characteristics of the filters and provide a valuable benchmark for model development.

Each set of experiments was conducted continuously until the filter reached the ultimate pressure drop (i.e., the failure threshold), ensuring the complete collection of data from the initial state to the failure of the filter.

A Hydrotechnik 3403-15-C3.39 pressure sensor was employed in the experiment to record the pressure drop across the test filter in real time at a sampling frequency of 5 Hz.

Table I. Experimental condition configuration

Experiment type	No.	Flow rate (L/min)	Temperature (°C)	Concentration (mg/L)
Temperature[27]	1	70	40	1
	2	70	30	1
	3	70	50	1
Flow rate[26]	1	70	40	1
	4	30	40	1
	5	50	40	1
	6	60	40	1
Concentration[28]	1	70	40	1
	7	70	40	0.25
	8	70	40	0.5
	9	70	40	1.5

Note that the condition of experiments No. 1 was chosen as a standard condition, which was compared in temperature flow rate and concentration experiments.

B. APDF MODEL PARAMETER SETTINGS

The APDF model was developed and implemented on the Python platform using the Keras deep learning framework. The model training was performed on a computer equipped with an Intel i7-9700 processor (3.00 GHz), 32 GB RAM, and an NVIDIA GeForce RTX 2060 GPU.

The details of LSTM network set were illustrated in Table II, including design of training epochs, batch size, dropout rate, LSTM network structure, initial learning rate, and adaptive learning rate strategy.

The input layer of the LSTM network model has three feature dimensions: the filter cake porosity ε, thickness L, and the effective filtration area ratio a. The hidden layer employs a three-layer LSTM structure, with the number of neurons decreasing layer by layer (256,128,64). A dropout layer is added after each LSTM layer, with a dropout rate set to 0.2, to prevent model overfitting. The output layer predicts the pressure drop for future consecutive time steps. The Adam optimizer is used, combined with early stopping and dynamic learning rate decay strategies, to balance training efficiency and convergence stability.

It is worth noting that only the degradation stage is involved in the training and prediction of model. During the healthy stage, the pressure drop remains largely stable without significant fluctuations. Consequently, the features in this stage do not contribute meaningfully to the prediction of oil filter degradation.

Table II. Neural network parameters

Parameter category	Parameter	Value
Sequence	Input sequence length	10
	Batch size	64
LSTM architecture	Input layer	3
	Hidden layer	256, 128, 64
	Output layer	1
	Dropout rate	0.2
Training	Training epochs	1000
	Learning rate η	0.001
	Learning rate γ,τ	0.0001

C. EXPERIMENT DESIGN

Several comparative models were constructed under consistent parameter settings: (1) the traditional LSTM model [15], which uses only historical pressure drop data as input; (2) the LSTM + MLP model [32], which also uses historical pressure drop data as input but introduces an additional MLP layer to extract working condition features; (3) the LSTM model with physics-inspired input (LSTM + PI), where the input features are obtained through a physical feature extraction layer but without physics loss function; (4) the APDF model, which not only processes the inputs through the physical feature extraction layer but also introduces a physics loss function; and (5) the purely physics model, extended Ergun model [13].

To analyze the impact of training data size on model performance, the APDF model was evaluated under varying training data proportions, as specified in Table III. The training and testing datasets were divided in chronological order.

To evaluate the impact of physical information on model performance and the advantages of the proposed adaptive weight design, we assigned different physical weights for testing and compared them with the proposed adaptive weight strategy. Detailed parameters are provided in Table IV.

IV. RESULT AND DISCUSSION

This section first presents the prediction performance of the proposed APDF model and its comparison with other methods. Then, the impacts of training data size and physical weight settings on model performance are analyzed, and the effectiveness of the adaptive weight design are discussed.

Table III. Training data parameters

Parameter	Value (%)
Training data size	40, 45, 50, 55

Table IV. Loss function weight parameters

Parameter	Value
Weight	0.1,0.2,0.3,0.4,0.5,0.6,0.7,0.8,0.9

A. THE PREDICTION PERFORMANCE OF APDF ON AVIATION HYDRAULIC FILTER

To intuitively demonstrate the performance of the APDF model in predicting the health status of aviation hydraulic filter, Fig. 4 presents a case study using the complete dataset (including nine working conditions) with a training data size of 50%.

As shown in Fig. 4, the prediction curve of the APDF model (red dashed line) closely aligns with the measured data (blue line). Meanwhile, the confidence interval effectively covers the majority of the measured data points, indicating that the proposed model exhibits not only strong predictive accuracy but also high robustness and reliability in assessing the health status of aviation hydraulic filters.

Furthermore, under the operating condition of a flow rate of 70 L/min, a temperature of 40 °C, and a contaminant concentration of 1.5 mg/L, the prediction performances of different models, including the LSTM model [15], the LSTM + MLP model [32], the LSTM + PI model, the APDF model, and the Ergun model [13], were compared with a training data size of 50%.

As shown in Fig. 5, the performances of APDF, LSTM + MLP, LSTM + PI, and Ergun models are better than that of LSTM model at the beginning of prediction. The LSTM + MLP model tends to overestimate the pressure drop rate, while the Ergun model underestimates it. The LSTM + PI model initially overestimates the pressure drop but gradually shifts to an underestimation in the later stage. In contrast, the APDF provides the best prediction, with its curve closely matching the true values throughout the entire time range.

The inferior performance of the LSTM model may be attributed to its inability to accurately capture the feature of exponential growth in the early degradation stage, where pressure drop changes are relatively small. LSTM + MLP model combines the temporal modeling capability of LSTM with the feature extraction strength of MLP. The prediction accuracy is improved, but it is still limited, especially during the later degradation stage. Inspired by the physical information, the LSTM + PI model processes

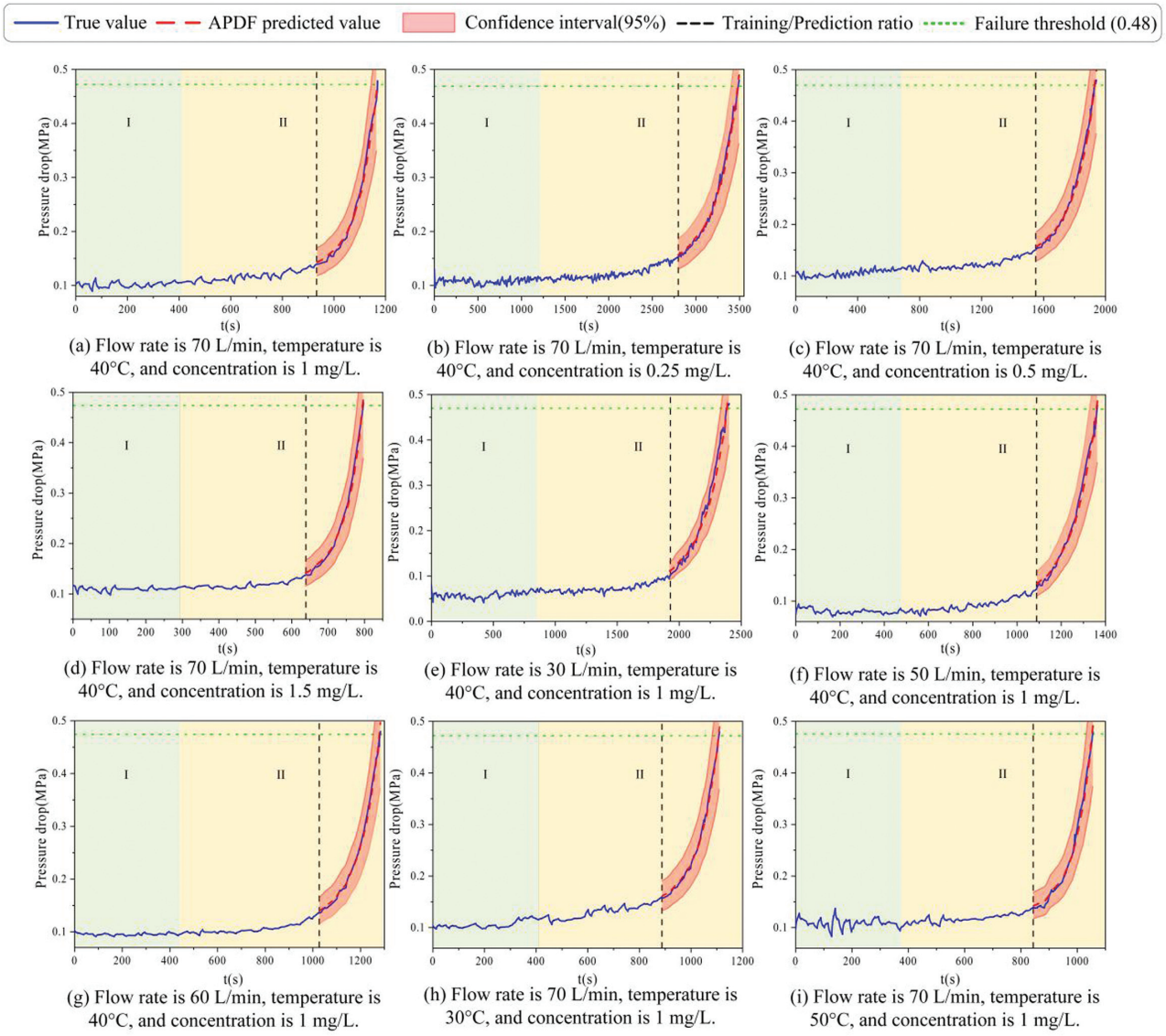

Fig. 4. The predictive performance of APDF model under different working conditions. I and II represent the healthy stage and the degradation stage, respectively. Only the degradation stage is involved in the training and prediction of model.

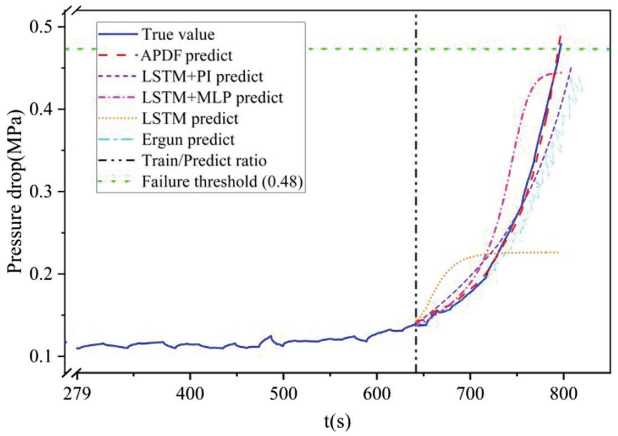

Fig. 5. Performance of different prediction models. The figure only displays the data from the degradation phase, as the data from the healthy phase were removed since it is not involved in training and prediction.

the inputs through the physical feature extraction layer which improves the feature representation and enhances prediction accuracy. However, the model still exhibits bias. The Ergun-based model combines the classical Ergun equation with a particle filtering framework, offering physically interpretable predictions. Although it successfully captures the general trend of pressure drop, its performance degrades during the later stages. This is largely due to its limited adaptability to highly nonlinear and rapidly changing system behavior.

In contrast, the proposed APDF model exhibits superior predictive performance. By deeply integrating physical information into the learning process, APDF can more accurately and effectively predict the pressure drop, particularly during the critical degradation phase.

To quantify the performance of different models above, root mean squared error (RMSE), mean absolute error (MAE), and the coefficient of determination (R^2) are applied. As shown in Table V, the RMSE of APDF is 0.0097 MPa, which is reduced by 87.6%, 79.9%, 65.0%, and 83.8% compared to the traditional LSTM (0.0789 MPa), the LSTM + MLP combined model (0.0481 MPa), the LSTM + PI model (0.0277 MPa), and the Ergun equation model (0.0600 MPa), respectively.

It demonstrates that the predictive accuracy of APDF surpasses other models by effectively integrating the physical information from the Ergun equation. This trendency also appeared in MAE and R^2 metric. The MAE and R^2 values of the proposed APDF model are 0.0074 MPa and 0.9963, respectively. Compared to the Ergun model (0.0448 MPa, 0.7163), the MAE error is reduced by approximately 83.6%, and the R^2 is improved by 39.1%. Additionally, in terms of training time, the training time of the APDF model (64.74 s) further validates its applicability in practical engineering, compared to traditional LSTM (196.93 s), LSTM + MLP (111.60 s), LSTM + PI (101.36 s), and the Ergun model (370.38 s), and its training time is significantly reduced by approximately 67.11%, 41.96%, 36.12%, and 82.52%, respectively.

Results above indicate that the APDF model can achieve superior prediction results within a shorter training time, greatly optimizing the computational resources and time costs required for model training in engineering applications.

B. PERFORMANCE OF APDF WITH DIFFERENT TRAINING SIZES

The training dataset size has a great impact on the prediction accuracy for the data-driven method. We further compared the prediction accuracy of hydraulic filter pressure drop of models such as APDF, LSTM, LSTM + MLP, and LSTM + PI, under different training data sizes for the working condition of 70 L/min flow rate, 40°C temperature, and 1.5 mg/L contaminant concentration.

Figure 6 demonstrates the violin plot of the absolute error distribution for LSTM, LSTM + MLP, LSTM + PI, and the proposed APDF model, under increasing training sizes from 40% to 55%. Each violin plot combines kernel density estimation with summary statistics to represent both the shape and spread of the error distribution. The red horizontal lines represent the mean error values. The color of each violin corresponds to a specific training size.

It can be observed that the absolute errors of all models decrease as the training data size increases. However, differences in distribution can be observed noticeably across models. The LSTM model generally shows wider distributions and higher error values, especially at lower training data sizes. The LSTM + MLP model demonstrates

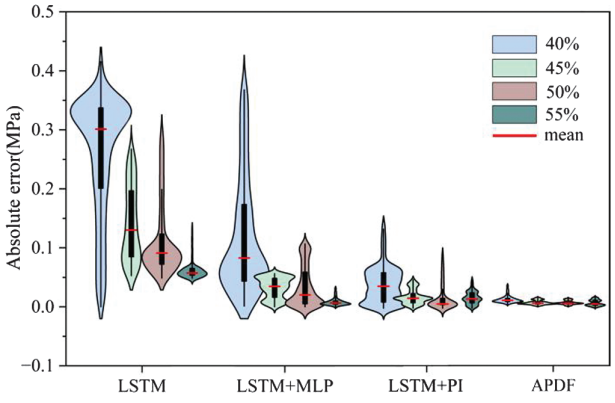

Fig. 6. Performance of different models on pressure drop prediction under various training data sizes.

Table V. Errors under different prediction models

	Prediction model				
Error	**LSTM**	**LSTM + MLP**	**LSTM + PI**	**Ergun**	**APDF**
RMSE (MPa)	0.0789	0.0481	0.0277	0.0600	0.0097
MAE (MPa)	0.0637	0.0339	0.0231	0.0448	0.0074
R^2	0.1389	0.7486	0.9015	0.7163	0.9963
Training time (s)	196.93	111.60	101.36	370.38	64.74

Table VI. RMSE of different models under various training data sizes

Model	Training data size(%)			
	40	45	50	55
LSTM	0.1222	0.1225	0.0789	0.0311
LSTM + MLP	0.1109	0.0986	0.0481	0.0152
LSTM + PI	0.0487	0.0371	0.0277	0.0159
APDF	0.0153	0.0124	0.0097	0.0076

slightly narrower error distributions than LSTM. Nevertheless, under smaller training data sizes, the distributions remain relatively wide and irregular. The LSTM + PI model shows improvements compared to the LSTM and LSTM + MLP models, but it still exhibits a relatively wide distribution and higher error values. The APDF model displays relatively compact and symmetric distributions across all training data sizes, with both the mean and median lines located consistently near lower error values.

It can be conclude that compared with pure data-driven models, APDF can show greater superiority when the amount of available training data is small. This might be attributed to that more physical mechanism leading to less reliance on data.

To quantify the performance of different models above, Table VI shows the RMSE of different prediction models under increasing training data sizes from 40% to 55%. At the 40% training data size, the prediction error of APDF (0.0153 MPa) is significantly lower than that of LSTM (0.1222 MPa), LSTM + MLP (0.1109 MPa), and LSTM + PI (0.0487 MPa). When the training data size is increased to 55%, although all models achieve significant reductions, the APDF model still maintained absolute superiority, with its RMSE (0.0076 MPa) showing a further 50% reduction compared to the LSTM + MLP (0.0152 MPa).

It is noteworthy that APDF model demonstrates particularly outstanding performance under limited data conditions. As 40% training data size, the error level is already close to the accuracy of the LSTM + MLP and LSTM + PI models with 55% training data size. This indicates that APDF model enhances the information extraction efficiency of the data by approximately 1.375 times by embedding physical laws. Furthermore, as the training data size increases, the error of the APDF model continues to decrease. Specifically, for every 5% increase in training data, the RMSE decreases by an average of 21.9%. This phenomenon argues that the physical constraint mechanism and data growth have a synergistic enhancement effect.

C. PERFORMANCE OF APDF UNDER ADAPTIVE PHYSICAL WEIGHT

In this study, physical information is integrated into the loss function by the adaptive weight of the physical term. To test the effectiveness of the adaptive weight design, two steps were conducted under the working condition of a flow rate of 70 L/min, a temperature of 40 °C, and a contaminant concentration of 1.5 mg/L: (1) the APDF with different fixed physical weights (denoted as PDF) were tested to investigate the influence of the weights on prediction performance; and (2) the PDF with best-performing weight was compared with the proposed adaptive weighting approach.

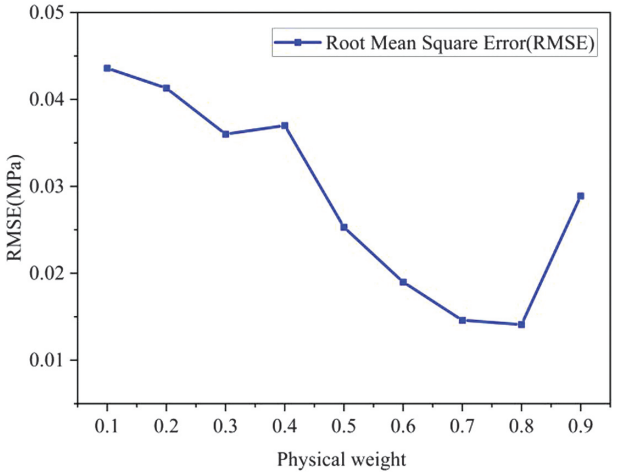

Fig. 7. Performance of PDF under different physical weights.

Figure 7 illustrates the performance of PDF with different physical weights. When the physical weight increases gradually from 0.1 to 0.8, the RMSE of the PDF model decreases progressively, indicating that enhancing the physical information can effectively improve the prediction accuracy. However, it is worth noting that as the physical weight exceeds 0.8, the RMSE of the PDF model begins to increase, which suggests that excessive reliance on physical information can degrade prediction performance.

That is to say, an overly high or overly low physical weight is not advantageous for pressure drop prediction. When the physical weight is too low (e.g., 0.1), the model relies excessively on data while neglecting the constraints of physical information, resulting in reduced prediction accuracy. In contrast, when the physical weight is too high (e.g., 0.9), the model becomes overly constrained by the physical information, limiting its ability to fully use of the available data and reducing its flexibility. Therefore, an appropriate balance between physical constraints and data-driven learning is crucial for optimizing model performance.

Figure 8 presents a performance comparison between the best-performing fixed-weight PDF and the proposed APDF model with adaptive weight design. It can be

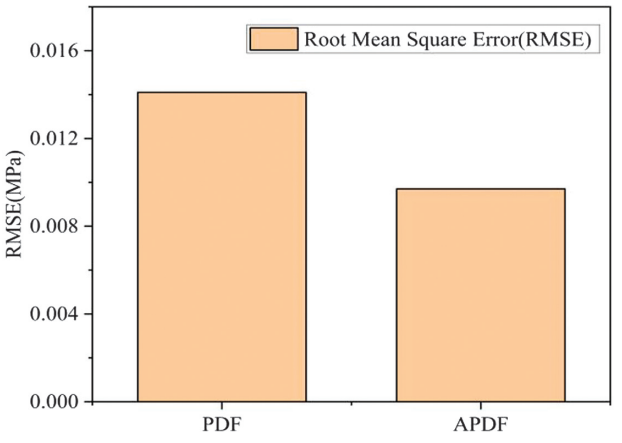

Fig. 8. Comparison of predictive performance between best-performing fixed-weight PDF and APDF.

observed that the fixed-weight PDF achieves an RMSE of 0.0141 MPa, while the APDF further reduces the error to 0.0097 MPa, demonstrating significant improvement in prediction performance.

This indicates that the adaptive weighting strategy effectively improve accuracy by automatically adjusting the contribution of physical terms during training. Such dynamic adjustment enables the model to maintain a more appropriate balance between physical consistency and learning flexibility, thereby enhancing prediction accuracy without requiring manual hyperparameter selection.

V. CONCLUSION

This study develops an APDF model to address the challenges in hydraulic filter health status prediction caused by nonlinear and individual variability degradation characteristics and limited data availability. APDF achieves deep fusion of physical knowledge and data-driven learning. Experimental results obtained from a hydraulic filter degradation experiment bench confirm that:

(1) Superior accuracy: the APDF model achieves an RMSE of 0.0097 MPa, representing reductions of 87.6%, 79.9%, 65.0%, and 83.8% compared to the LSTM (0.0789 MPa), LSTM + MLP (0.0481 MPa), the LSTM + PI model (0.0277 MPa), and physics-driven Ergun model (0.0600 MPa), respectively.

(2) Efficient data utilization: under a limited data scenario with 40% training data, the APDF delivers prediction performance comparable to traditional models trained with 55% of the data, demonstrating its strong generalization capability under data-constrained conditions.

(3) Effectiveness of the adaptive physical-weight design: By dynamically adjusting the contribution of the physical constraint during training, the APDF model achieves an RMSE of 0.0097 MPa, outperforming the best fixed-weight PDF (0.0141 MPa) and thus demonstrating a substantial enhancement in prediction accuracy.

It is worth noting that although the proposed APDF model demonstrates strong prediction accuracy and robustness under limited data conditions, several issues still deserve further investigation. In the present study, the degradation experiments were conducted under relatively fixed operating conditions, whereas actual aircraft hydraulic systems usually operate under dynamically varying conditions. Therefore, future work will focus on extending the proposed framework to more complex and time-varying operating environments to further improve its engineering applicability. In addition, the proposed APDF strategy also has the potential to be generalized to other prognostics and health management (PHM) tasks in aerospace systems, such as pumps, actuators, and servo valves.

ACKNOWLEDGMENTS

This research was supported by grants from the National Natural Science Foundation of China (52205065) and the Shanxi Province Basic Research Program Joint Funding Project (202403011212005).

DATA AVAILABILITY STATEMENT

Data will be made available on request.

CONFLICT OF INTEREST STATEMENT

The authors declare that they have no conflicts of interest related to this work.

REFERENCES

[1] Z. Song, Y. W. Feng, and C. Lu, "Superimposable neural network for health monitoring of aircraft hydraulic system," *Eng. Fail. Anal.*, vol. 160, p. 108063, 2024.

[2] N. Novak *et al.*, "Degradation of hydraulic system due to wear particles or medium test dust," *Appl. Sci.*, vol. 13, no. 13, p. 7777, 2023.

[3] F. Ng, J. A. Harding, and J. Glass, "Improving hydraulic excavator performance through in line hydraulic oil contamination monitoring," *Mech. Syst. Signal Pr.*, vol. 83, pp. 176–193, 2017.

[4] G. Sorrentino, K. Chellappah, and G. Biscontin, "Understanding clogging mechanisms in filter media: An integration of laboratory findings and theoretical perspectives," *Sep. Purif. Technol.*, vol. 359, p. 130602, 2024.

[5] Y. Wang *et al.*, "Prediction of diesel particulate filter regeneration conditions and diesel engine performance under regeneration mode using AMSO-BPNN and combined with XGBoost," *Appl. Energy*, vol. 377, p. 124341, 2025.

[6] K. Rui, G. Wenjun, and C. Yunxia, "Model-driven degradation modeling approaches: Investigation and review," *Chin. J. Aeronaut.*, vol. 33, no. 4, pp. 1137–1153, 2020.

[7] H. Li *et al.*, "A review on physics-informed data-driven remaining useful life prediction: Challenges and opportunities," *Mech. Syst. Signal Pr.*, vol. 209, p. 111120, 2024.

[8] S. Yang *et al.*, "Industrial battery state-of-health estimation with incomplete limited data toward second-life applications," *JDMD*, vol. 3, no. 4, pp. 246–257, 2024.

[9] E. Vanem *et al.*, "Statistical models for condition monitoring and state of health estimation of lithium-ion batteries for ships," *JDMD*, vol. 3, no. 1, pp. 11–20, 2024.

[10] N. Vernikovskaya *et al.*, "Filtration of the catalyst suspension in hydrogenated oil through the woven cloth: Mathematical model of the process accounting for dynamics of the cake growth and filter pore blockage," *Sep. Purif. Techno.*, vol. 212, pp. 355–367, 2019.

[11] M. Rehman, M. B. Hafeez, and M. Krawczuk, "A comprehensive review: Applications of the Kozeny–Carman Model in engineering with permeability dynamics," *Arch. Comput. Method E.*, vol. 31, no. 7, pp. 3843–3855, 2024.

[12] I. F. Macdonald *et al.*, "Flow through porous media-the Ergun equation revisited," *Ind. Eng. Chem. Fundam.*, vol. 18, no. 3, pp. 199–208, 1979.

[13] O. F. Eker, F. Camci, and I. K. Jennions, "Physics-based prognostic modelling of filter clogging phenomena," *Mech. Syst. Signal Pr.*, vol. 75, pp. 395–412, 2016.

[14] Z. Wang *et al.*, "Knowledge and data jointly driven aero-engine gas path performance assessment method," *Chin. J. Aeronaut.*, vol. 37, no. 5, pp. 533–557, 2024.

[15] Y. Hu *et al.*, "Performance degradation prediction using LSTM with optimized parameters," *Sensors*, vol. 22, no. 6, p. 2407, 2022.

[16] J. Chen *et al.*, "Gated recurrent unit based recurrent neural network for remaining useful life prediction of nonlinear deterioration process," *Reliab. Eng. Syst. Safe*, vol. 185, pp. 372–382, 2019.

[17] S. Lee *et al.*, "Data-driven health condition and RUL prognosis for liquid filtration systems," *J. Mech. Sci. Technol.*, vol. 35, no. 4, pp. 1597–1607, 2021.

[18] L. Tiltmann, Neural Networks for Predicting Fluid Filter Remaining Useful Life [dissertation]. Gothenburg (SE): Chalmers University of Technology; 2025.

[19] J. Xia *et al.*, "Digital twin-assisted fault diagnosis of rotating machinery without measured fault data," *TIM*, vol. 73, pp. 1–10, 2024.

[20] C. Xu *et al.*, "Photocatalytic and filtration performance study of TiO2/CNTs-filter for oil particle," *Process Saf. Environ.*, vol. 123, pp. 72–78, 2019.

[21] Y. Zhu *et al.*, "Domain generalization prognosis method for lithium-ion battery state of health with transformer and multi-kernel MMD," *JDMD*, vol. 3, no. 4, pp. 311–323, 2024.

[22] X. Li *et al.*, "A single-device environment-adaptive mixed reality framework for real-time industrial fault diagnosis," *JDMD*, vol. 5, no. 1, pp. 64–73, 2026.

[23] S. Kohtz *et al.*, "Physics-informed machine learning model for battery state of health prognostics using partial charging segments," *Mech. Syst. Signal Pr.*, vol. 172, p.109002, 2022.

[24] M. Rosenkranz *et al.*, "Viscoelasticty with physics-augmented neural networks: Model formulation and training methods without prescribed internal variables," *Comput. Mech.*, vol. 74, no. 6, pp. 1279–1301, 2024.

[25] L. G. Wright *et al.*, "Deep physical neural networks trained with back propagation," *Nature*, vol. 601, no. 7894, pp. 549–555, 2022.

[26] J. Hao *et al.*, "The pressure drop of fibrous surface filters for gas Filtration: Modeling and experimental studies," *Sep. Purif. Technol.*, vol. 350, p. 127981, 2024.

[27] Y. Yu *et al.*, "A review of recurrent neural networks: LSTM cells and network architectures," *Neural Comput.*, vol. 31, no. 7, pp. 1235–1270, 2019.

[28] S. D. Iyaghigba, I. Petrunin, and N. P. Avdelidis, "Modeling a hydraulically powered flight control actuation system," *Appl. Sci.*, vol. 14, no. 3, p. 1206, 2024.

[29] M. A. R. Adli, "Analysis of aircraft hydraulic filter flow: Computational fluid dynamics simulation using simflow 4.0," *Adv. Sustain. Technol. (ASET)*, vol. 3, no. 2, pp. 42–50, 2024.

[30] L. I. U. Haodong *et al.*, "Simulation of an aircraft thermal management system based on vapor cycle response surface model," *Chin. J. Aeronaut.*, vol. 37, no. 6, pp. 64–77, 2024.

[31] R. Zhang *et al.*, "Active control of hydraulic oil contamination to extend the service life of aviation hydraulic system," *Int. J. Adv. Manuf. Tech.*, vol. 96, pp. 1693–1704, 2018.

[32] M. Cordeiro-Costas *et al.*, "NSGA-II based short-term building energy management using optimal LSTM-MLP forecasts," *Int. J. Electr. Power Energy Syst.*, vol. 159, p. 110070, 2024.